ARL-TR-8808 ● SEP 2019

# Improved Low-Velocity Impact Performance of the Advanced Combat Helmet (ACH) at 17 ft/s through Optimization of Pad Material Response

by Jeffrey Staniszewski, Matthew Walter, and Thomas Plaisted

## NOTICES

### Disclaimers

The findings in this report are not to be construed as an official Department of the Army position unless so designated by other authorized documents.

Citation of manufacturer's or trade names does not constitute an official endorsement or approval of the use thereof.

Destroy this report when it is no longer needed. Do not return it to the originator.

ARL-TR-8808 ● SEP 2019


# Improved Low-Velocity Impact Performance of the Advanced Combat Helmet (ACH) at 17 ft/s through Optimization of Pad Material Response

**Jeffrey Staniszewski and Thomas Plaisted**
*Weapons and Materials Research Directorate, CCDC Army Research Laboratory*

**Matthew Walter**
*Bennett Aerospace, Inc., Cary, NC*

# REPORT DOCUMENTATION PAGE

*Form Approved*
*OMB No. 0704-0188*



| 1. REPORT DATE *(DD-MM-YYYY)* | 2. REPORT TYPE | 3. DATES COVERED (From - To) |
|---|---|---|
| September 2019 | Technical Report | March 2018–May 2019 |

**4. TITLE AND SUBTITLE**
Improved Low-Velocity Impact Performance of the Advanced Combat Helmet (ACH) at 17 ft/s through Optimization of Pad Material Response

**5a. CONTRACT NUMBER**

**5b. GRANT NUMBER**

**5c. PROGRAM ELEMENT NUMBER**

**6. AUTHOR(S)**
Jeffrey Staniszewski, Matthew Walter, and Thomas Plaisted

**5d. PROJECT NUMBER**

**5e. TASK NUMBER**

**5f. WORK UNIT NUMBER**

**7. PERFORMING ORGANIZATION NAME(S) AND ADDRESS(ES)**
CCDC Army Research Laboratory
ATTN: FCDD-RLW-MA
Aberdeen Proving Ground, MD 21005

**8. PERFORMING ORGANIZATION REPORT NUMBER**
ARL-TR-8808

**9. SPONSORING/MONITORING AGENCY NAME(S) AND ADDRESS(ES)**

**10. SPONSOR/MONITOR'S ACRONYM(S)**

**11. SPONSOR/MONITOR'S REPORT NUMBER(S)**

**12. DISTRIBUTION/AVAILABILITY STATEMENT**
Approved for public release; distribution is unlimited.

**13. SUPPLEMENTARY NOTES**
ORCID IDs: Jeffrey Staniszewski, 0000-0002-2469-3257; Matthew Walter, 0000-0002-1237-2843; Thomas Plaisted, 0000-0003-2903-3263.

**14. ABSTRACT**
Soldiers may be subjected to potential head injury from blunt impact and ballistic threats in a wide variety of training and battlefield scenarios. The Advanced Combat Helmet (ACH) is designed to protect the head from injury against these threats. The ACH, consisting of the outer shell, suspension system, and retention system, protects against injury from blunt impact by limiting headform accelerations during impact testing at 10 ft/s to below 150 g. This study investigated the potential for performance enhancements at higher impact velocities through modification of the suspension system, which is the padding on the interior of the helmet. A low-velocity impact model of the ACH previously validated across several velocities and impact locations was used to study the influence of assumed pad response on the predicted peak headform acceleration during blunt impact testing at 17 ft/s. Headform accelerations were minimized to below 150 g for four of the five testing impact locations by optimizing the compressive response of the individual pads in the suspension system. Comparisons between manual and software-based optimization strategies are presented that illustrate the advantages of iterative optimization algorithms. This work provides a guideline for selecting ACH padding to limit the severity of head injury resulting from blunt force impact.

**15. SUBJECT TERMS**
head injury, blunt impact protection, helmet suspension, optimization, combat helmet, finite element analysis

| 16. SECURITY CLASSIFICATION OF: | | | 17. LIMITATION OF ABSTRACT | 18. NUMBER OF PAGES | 19a. NAME OF RESPONSIBLE PERSON |
|---|---|---|---|---|---|
| a. REPORT | b. ABSTRACT | c. THIS PAGE | | | Jeffrey Staniszewski |
| Unclassified | Unclassified | Unclassified | UU | 36 | 19b. TELEPHONE NUMBER (Include area code) 410-306-0807 |

## Contents

## List of Figures

## List of Tables

## Acknowledgments

The authors acknowledge the US Army Combat Capabilities Development Command (CCDC) Soldier Center for funding this research through Project 18-211. The research reported in this document was performed in connection with contract/instrument W911QX-16-D-0014 with the US Army Research Laboratory. (As of 31 January 2019, the organization is now part of CCDC [formerly RDECOM] and is now called CCDC Army Research Laboratory [ARL].) The views and conclusions contained in this document are those of Bennett Aerospace and ARL. Citation of manufacturer's or trade names does not constitute an official endorsement or approval of the use thereof. The US government is authorized to reproduce and distribute reprints for government purposes notwithstanding any copyright notation hereon.

# 1. Introduction

Prevention of head injury due to blunt impact is an increasing concern for the military as well as for athletics and the broader society. Strategies to mitigate head injury, particularly brain injury, seek to minimize head acceleration through engineered helmet suspension systems. Suspension systems often take the form of foam or elastomeric padding, designed to compress under impact, reducing the peak acceleration and effectively extending the duration of loading to the head.[1] Pneumatic padding or textile based sling suspension systems are also used.[2,3] The space between the head and interior of the helmet shell, where the suspension system must perform, is typically limited to achieve other performance metrics, such as minimized system weight and offset distance from the center of gravity of the head, as well as achieving a comfortable fit for the wearer. The suspension system must be carefully tuned to balance these competing demands while providing the maximum amount of blunt impact protection.

The ACH is evaluated for blunt impact performance per Section 4.10.13 – *Blunt Impact Performance of the ACH Purchase Description*,[4] which calls for helmet impact testing according to Department of Transportation (DOT) *Federal Motor Vehicle Safety Standard (FMVSS) 218* with modifications specific to military helmets.[5] The testing standard involves placing a complete Advanced Combat Helmet (ACH), consisting of the outer shell, suspension system, and retention system (chin strap and hardware), on an instrumented magnesium headform. The testing detailed in this document is conducted with an ACH, size large, on a DOT Type C headform. The headform and helmet assembly is dropped from elevation, guided by a monorail, such that impact occurs onto a rigid, stationary anvil with hemispherical shape at a prescribed velocity. The current standard requires that helmets must limit headform acceleration to less than 150 g (g-force, 9.81 $m/s^2$) for impacts at 10 ft/s. The impacts target specific areas of the helmet including the crown, front, rear, sides, and nape regions, as shown in Fig. 1. The ACH currently meets this performance standard with a seven-pad suspension system made of polyurethane foam detailed in the following section.

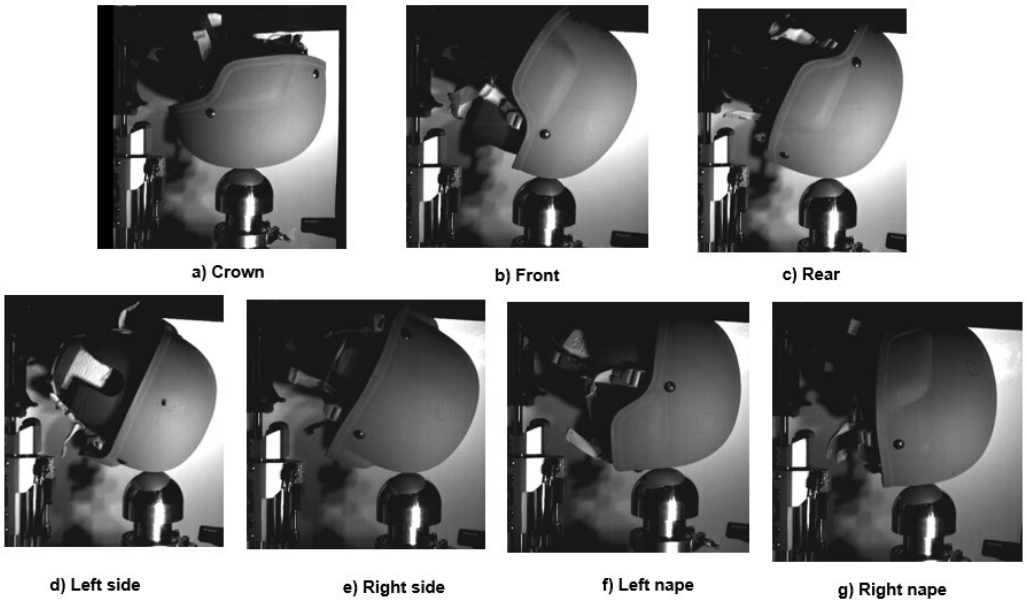


**Fig. 1 Helmet impact locations per DOT FMVSS 218**

Recommendations have been made to increase the blunt impact testing velocity to better reflect blunt trauma threats experienced by Soldiers in training and battlefield scenarios.[6] As an example, paratroopers regularly approach the ground during landing at velocities of 15–20 ft/s by design of the parachute system, though variable landing conditions can lead to even higher impact speeds. Given that within the paratrooper population there is a head injury incidence rate nearly twice that of the general population, additional head impact protection would be beneficial.[7] Increasing protection would either require significantly increasing the thickness of the current padding material, which comes at the expense of other performance tradeoffs, or engineering a new suspension system that maximizes the energy attenuation within the available space currently allocated inside the helmet.

Toward the goal of engineering a new suspension system, we use a computational model of the ACH helmet, referred to as the Low-Velocity ACH (LVACH) model, to determine optimized load deflection characteristics of the suspension system to protect against impacts velocities at 17 ft/s.[8] The LVACH model achieves good correlation to experimental blunt impact testing in terms of magnitude, phase, and shape of the headform acceleration versus time response for impacts to the crown, front, side, nape, and rear locations at impact velocities of 10, 14, and 17 ft/s. On a scale of 0 to 1, the average CORA (CORrelation and Analysis) score was 0.82 based upon 15 validation cases (five impact locations at three velocities), where 1 represents 100% correlation. The best correlation was achieved at 10 and 14 ft/s,

while at 17 ft/s the model can be considered conservative since it might overpredict peak headform accelerations, as shown in Fig. 2.

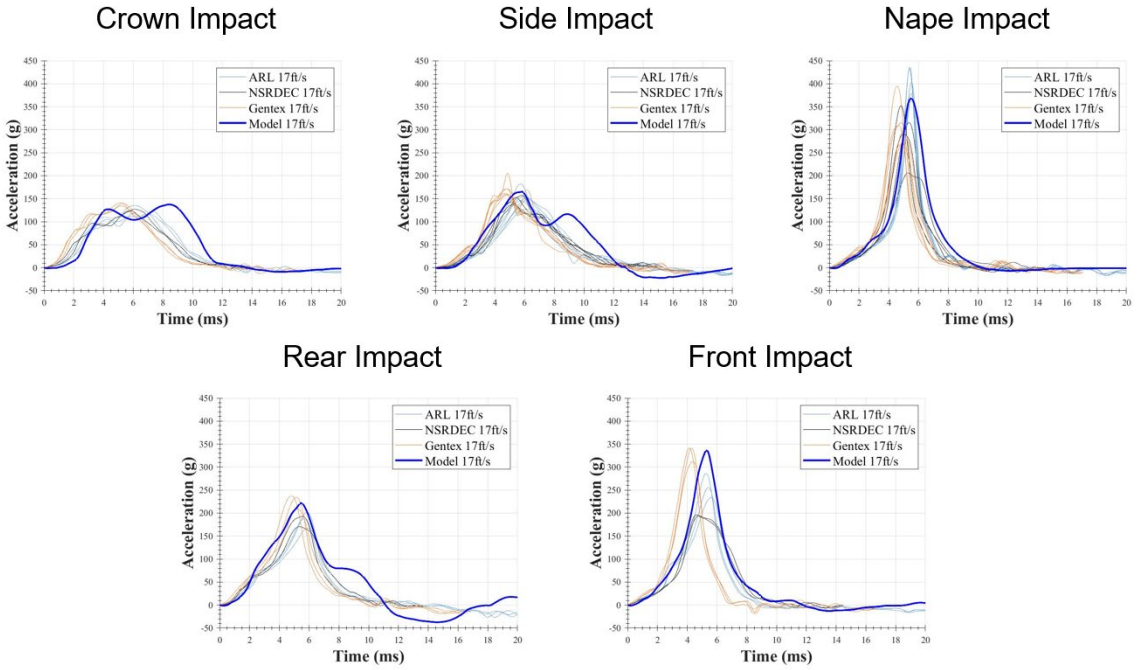


**Fig. 2 Headform acceleration for impacts at 17 ft/s: response of LVACH computational model (blue) compared with experimental responses from testing at various laboratories**

## 2. Problem Definition and Approach

The goal of this study is to determine a set of pad material characteristics for the ACH that reduce the peak headform acceleration below 150 g (pass/fail limit) during impact at 17 ft/s for all tested impact sites. The most straightforward approach to reducing headform accelerations would be to individually optimize the material response of the pad directly behind each impact location (i.e., optimizing the crown pad for only the crown impact scenario). Although simple, this approach ignores that fact that every pad participates, to some degree, in the response of the system at each impact location. As such, it is necessary to determine the influence of the individual pads to each impact location and optimize their material responses based on these interactions.

The pads supplied with the ACH are manufactured by Team Wendy under the trade name Zorbium Action Pad (ZAP) and consist of an assembly of an open-cell polyurethane foam with two layers of different density bonded together and encased in a sealed thermoplastic moisture barrier film. The assembly is then encased in a textile fabric cover. Experimental characterization of the compressive material

response of the ZAP pad assembly was previously conducted at impact velocities of interest, where the resulting compressive response is shown in Fig. 3.[8]

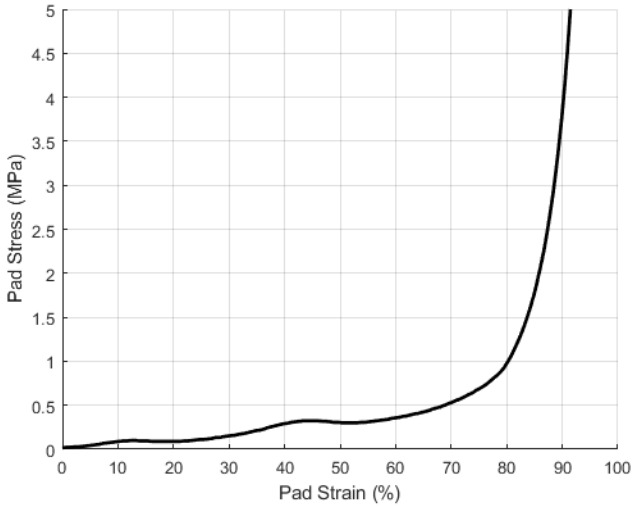


**Fig. 3 Experimental response of Team Wendy pad**

The full ZAP suspension system consists of seven pads, as shown in Fig. 4. The size and shape of each pad differs based on its location within the helmet, while their materials construction are uniform. Placement of the pads in the standard configuration shown in Fig. 4 is required for combat operations as well as blunt impact testing.[4,9] The crown pad is circular with a nominal dimension of 126 mm, the side and nape pads are oblong with dimensions of 86.5 × 49.5 mm, and the front and rear pads have a trapezoidal shape with dimensions of 82 × 88 and 78 × 88 mm, respectively. Each pad assembly, including a moisture barrier and fabric cover, has a thickness of 22 mm. The pads are modeled as a homogeneous material using the low-density foam material model (MAT_057) in LS-Dyna and are placed within the modeled helmet shell at positions corresponding to their configuration during impact testing. The thickness of the modeled pads is slightly thinner at 19 mm to reflect the thickness of the foam component, as the encasing moisture barrier and fabric cover are not explicitly modeled and have minimal effect on the material response.

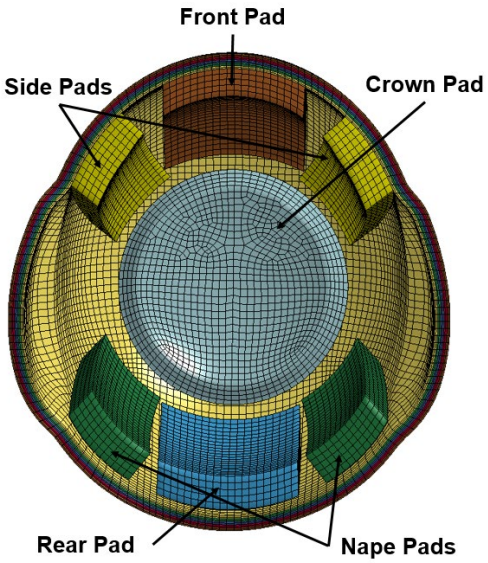


**Fig. 4. Interior view of ACH model**

As seen in the experimental results and predictions of 17 ft/s impacts shown in Fig. 2, modification of the pad material response is required to reduce headform accelerations to acceptable levels. Determination of a material response that significantly reduces headform accelerations is difficult because it is unknown which properties of the response could contribute to this objective. Additionally, infinite permutations in stress–strain behavior can be created as potential solutions. To bound the problem, a well-defined shape of compressive pad response is selected. It is assumed that the pad behaves like a theoretically ideal energy absorber with a response that is broken into three parts 1) a linear region with an initial modulus up to the yield stress, 2) a region where stress is constant at the yield stress while the pad is compressed up to its densification strain, and 3) a region after the densification strain where the stress increases significantly as a function of strain.[10] This material response can be described with four inputs: the initial modulus, yield stress, densification strain, and densification response. In this study, the amount of potential material responses is reduced by setting the densification strain to a constant 70% and prescribing a singular densification response. The two remaining inputs, the initial modulus $E_0$ and yield stress $\sigma_{ys}$, are initially varied between bounds of 5 and 33.3 MPa and 0.15 and 1.5 MPa, respectively. These bounds were chosen because they encompass the majority of available energy absorbing materials that could meet the mass requirements. Figure 5 shows the bounds of the potential pad responses that are explored in this analysis.

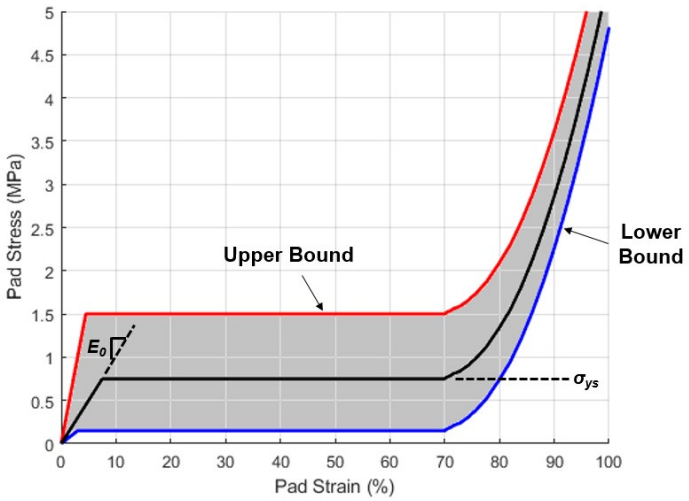


**Fig. 5 Initial design space for potential pad response**

An initial modulus and yield stress are defined for each of the five pad types (nape, rear, side, front, and crown), resulting in a total of 10 input parameters: $E_{0,n}$, $\sigma_{ys,n}$, $E_{0,r}$, $\sigma_{ys,r}$, $E_{0,s}$, $\sigma_{ys,s}$, $E_{0,f}$, $\sigma_{ys,f}$, $E_{0,c}$, and $\sigma_{ys,c}$. An optimal combination of input parameters is determined using a series of space filling designs. Using a Design of Experiments (DOE) approach, a 100-case Latin hypercube sampling of the 10-dimensional parameter space is created within the previously discussed initial bounds for modulus and yield stress. For each case in the design space, a MATLAB script creates a file to be included with the model input that contains a set of five curves to define each pad material response. All of the design cases are simulated for a chosen impact location and acceleration versus time curves of the headform are extracted. Results from peak headform accelerations are used to modify the upper and lower bounds of analyses on subsequent impact locations. The nape and rear impact locations are first used to establish a range of acceptable input parameters for the nape and rear pads. A subsequent 100-case space filling design is generated to investigate the crown and front pad parameters using their respective impact locations and the newly established bounds. Simulations of the side impact location are run with a third 100-case space filling design to determine optimal parameters for the side pad response. The results of this series of design studies is detailed in the following sections.

## 3. Nape and Rear Impact Results

The parametric study of pad material properties begins with the nape and rear impact locations for two major reasons. The influence of the nape and rear pad properties is largely isolated from the three remaining impact locations. Also, the nape impact location has the highest experimental and predicted headform

acceleration and thus the furthest from the prescribed limit of 150 g. Simulations of both the nape and rear impact locations were run for each design case in the 100-case space filling design and postprocessed to obtain peak headform accelerations. The initial design produced 19 nape impact simulations with a peak acceleration below 150 g, but only 2 rear impact simulations were below this limit. None of the design cases were below the 150 g for both impact locations. Figure 6 plots the relationship between the nape and the rear maximum accelerations for this initial design. An analysis of the maximum accelerations from each impact location revealed that the most influential input parameters were the yield stresses from the nape and rear pads. The results from the nape and rear impact locations in relation to the nape and rear yield stresses are shown in Fig. 7. These plots show that there is an interaction between the nape and rear yield stresses in relation to both maximum accelerations. For both impact locations, regions with accelerations that are close to passing the 150-g limit can be identified (although there is only a small area where these regions overlap).

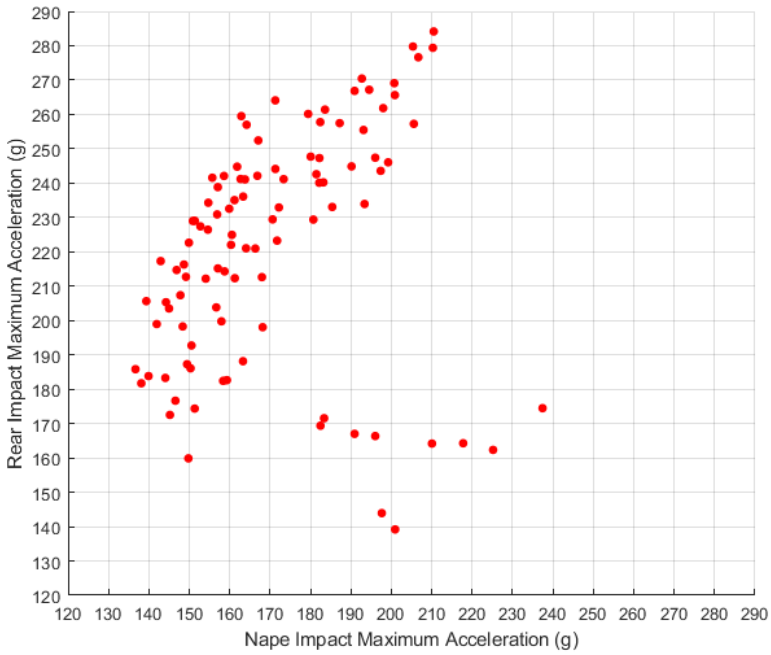


**Fig. 6 Maximum accelerations from nape and rear impact locations**

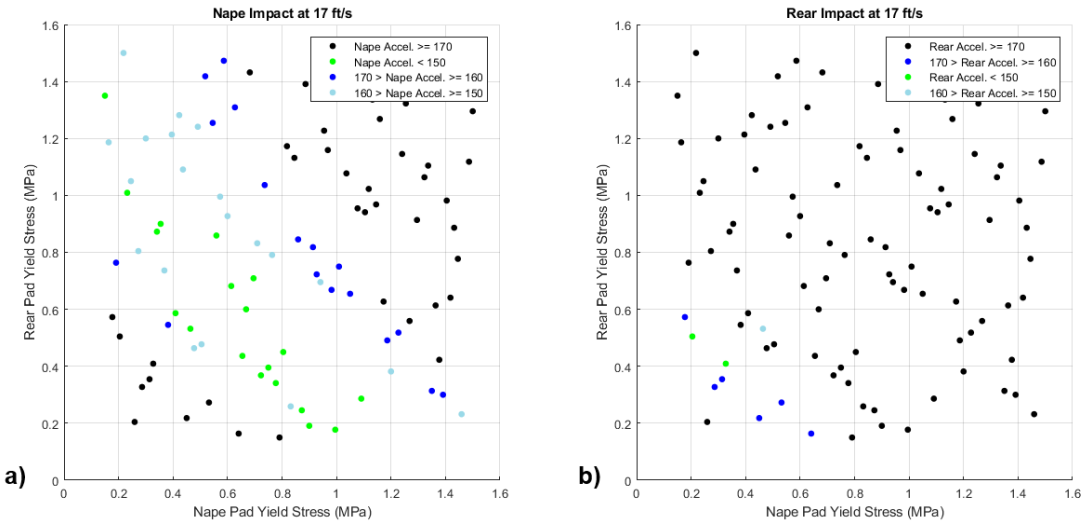


**Fig. 7 Results of a) nape and b) rear impacts in relation to nape and rear plateau stress values**

The portion near the origin of the two-parameter design space shown in Fig. 7 is the only area with the potential to reduce headform accelerations below the 150-g limit for both cases as it contains all the rear impact results below 170 g. The effects of the eight remaining input parameters on the rear impact response were also investigated to identify additional, potentially beneficial pad behavior. The relationship between the yield stress of the crown pad and the rear impact maximum acceleration plotted in Fig. 8 shows that the lowest headform accelerations are correlated with lower values of crown pad yield stress. This result, coupled with the information on the interaction between nape and rear yield stresses, is used to modify the parameter ranges of the pad response. The lower and upper bounds of the yield stress for the crown pad were set to 0.05 and 0.4 MPa, respectively. The selection of nape and rear yield stresses was restricted to a roughly triangular area in the two-parameter design space bounded by the lines $\sigma_{ys,n}$ = 0.15 MPa, $\sigma_{ys,r}$ = 0.15 MPa, and $\sigma_{ys,r} = 1.20 - \sigma_{ys,n}$ MPa, where $\sigma_{ys,n}$ and $\sigma_{ys,r}$ are the nape and rear pad yield stresses, respectively. The bounds for the yield stresses of the other pads and the initial moduli of all the pads remain unchanged.

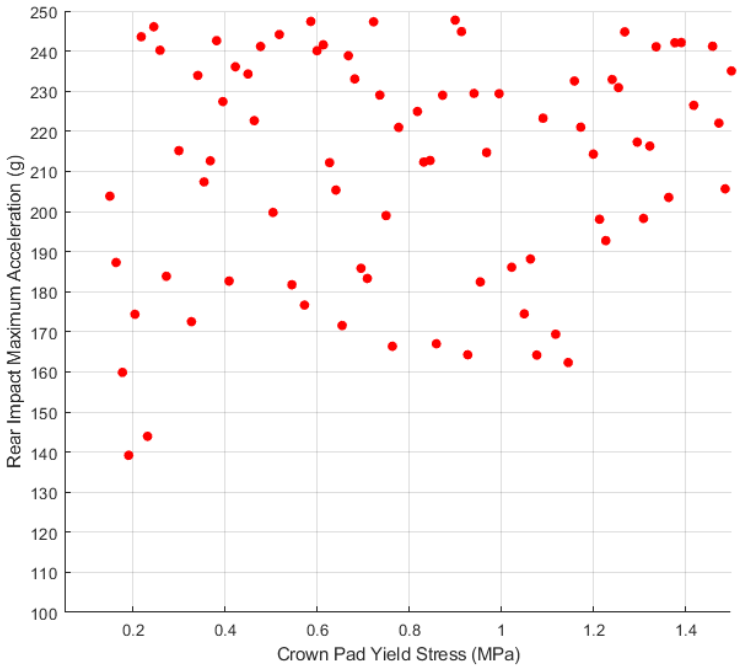


**Fig. 8 Maximum acceleration prediction of rear impact vs. crown pad yield stress**

A second 100-case space filling design is generated with the new parameter bounds, and simulations of nape and rear impact locations were completed and postprocessed. The lower crown yield stress coupled with the nape and rear yield stress relationship improved the overall response of the rear impacts, resulting in more cases that are below the 150-g limit. Results for the nape and rear maximum headform accelerations for this space filling design are shown in Fig. 9. Similar to the first iteration, none of the design cases resulted in maximum accelerations for both impact locations below the 150-g limit, although several cases have peak accelerations near or below 160 g for both cases. The predictions of peak headform accelerations for the baseline ACH model with Team Wendy pad properties were on the high end of the experimental values, so it can be suggested that actual experimental data for these cases may result in maximums below the 150-g limit. Further adjustments to the bounds of the nape and rear yield stresses are unlikely to improve the response for both impacts simultaneously. Conditions to significantly reduce the peak accelerations for the nape and rear impact locations have been established and optimization of the remaining pad properties for the three additional impact locations is the next objective.

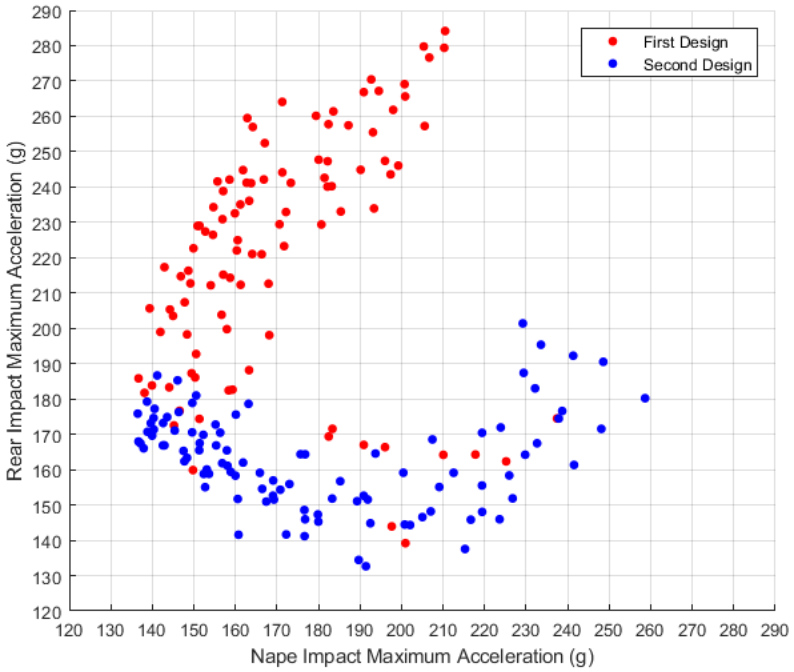


**Fig. 9 Combined results of maximum accelerations from nape and rear impact locations**

## 4. Crown and Front Impact Results

The crown impact was the next location to be studied because the property range of the crown pad was influenced by the rear impact response. Results from the baseline ACH model with Team Wendy pads have shown that the front pad is compressed during crown impact before the crown pad becomes engaged (Fig. 10). Investigation of the response from the front impact location is therefore coupled to the crown impact location, as the front pad response is likely influential for both cases. Crown and front impact simulations were run using the second iteration of the 100-case space filling design from the previous analysis of the nape and rear impact locations. The complete set of acceleration versus time curves for the crown impact are shown in Fig 11a, and those curves with peak values below 160 g are shown in Fig. 11b. Several cases for the crown impact are significantly below the 150-g limit, with the lowest peak acceleration being 109 g.

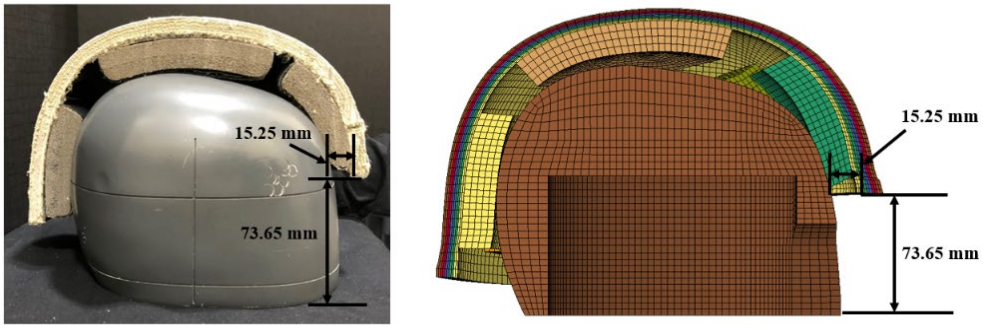


**Fig. 10 Pad positioning inside the ACH: experimental (left) and finite element model (right) indicate pad precompression of the front oblong pad**

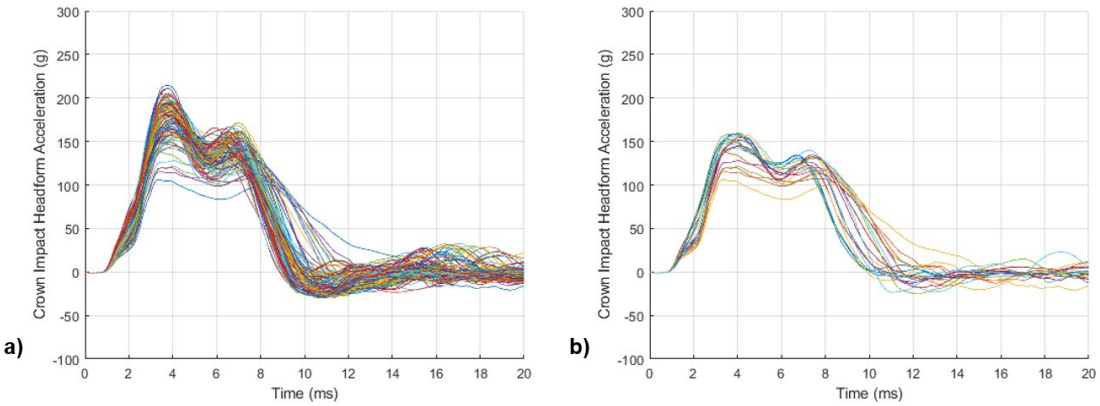


**Fig. 11 Acceleration vs. time curves for crown impact a) all 100 design cases and b) design case with peak accelerations less than 160 g**

Results from the front impact location in Fig. 12 show that all of the design cases have peak accelerations that are at least 180 g, with only three cases achieving a peak acceleration of less than 190 g. The high predicted peak accelerations for this location can be attributed to the positioning of the helmet on the headform. Experimental measurements of headform and helmet spacing, taken from the ACH helmet with Team Wendy padding, were used to position the headform within the modeled helmet shell. A gap of 15.25 mm between the interior of the front brim of the helmet and the front of the headform was measured from the experimental configuration and transferred to the model. This spacing causes the front pad, with an original thickness of 19 mm, to become partially compressed between the interior of the helmet shell and the front of the headform. Although the precompression of the pad does not cause initial stresses in the model, the smaller gap between the headform and interior surface of the helmet may be contributing to the difficulty of reducing peak accelerations. Changes to the initial gap spacing that could be caused by a pad material response that is different from the Team Wendy pad were not included in this analysis.

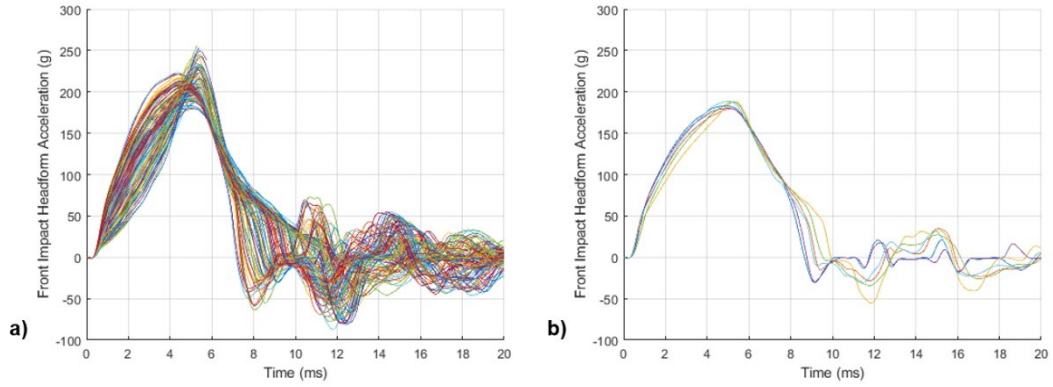


**Fig. 12 Acceleration vs. time curves for front impact of a) all 100 design cases and b) design case with peaks less than 190 g**

Figure 13 shows the effect of the front pad yield stress on the maximum headform accelerations of both the front and crown impact locations. Figure 13a shows that the front impact response is highly dependent on the assumed yield stress of the front pad, with maximum accelerations decreasing for increasing yield stress until approximately 1.1 MPa after which they slightly increase. The dependency on front pad yield stress for the crown impact location is less significant, as the crown pad also influences these results, although in Fig. 13b it is clear that values below 0.6 MPa are beneficial for this location. Optimizing the front pad yield stress will need to balance the benefits of a higher value for the front impact location with the reduction in maximum acceleration for the crown location. Modifications to the upper and lower limits of this parameter cannot be made due to these competing benefits.

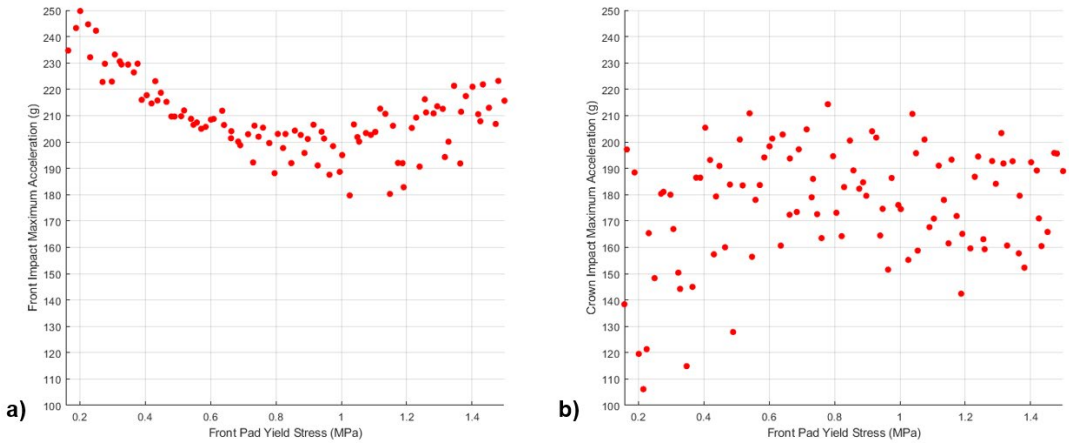


**Fig. 13 Effect of front pad yield stress on a) front impact and b) crown impact**

In addition to the front pad yield stress, the yield stress of the side pad is influential in the response of both the front and crown impact locations. Generally, the maximum acceleration from a front impact is lowered with a reduction in side pad

yield stress, as shown in Fig. 14a. Although the effect is not as significant, Fig. 14b also shows that the maximum accelerations from the crown impact decrease as side pad yield stresses are reduced. These results suggest that reducing both the lower and upper bounds of the side pad yield stress would improve the response for the crown and front impact locations without modifying those results from the nape and rear impacts. Before making these changes, it is important to examine the predictions from the side impact location to ensure it is not adversely affected by lower side pad yield stresses.

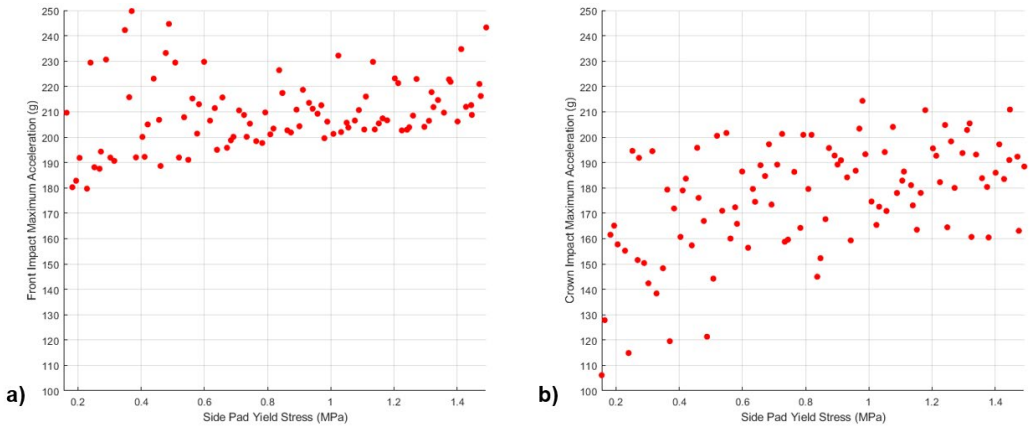


**Fig. 14 Effect of side pad yield stress on a) front impact and b) crown impact**

## 5. Side Impact Results

Predictions of maximum headform acceleration from the side impact location were run for the second iteration of the 100-case space filling design previously used for the other four impact locations. The predicted headform accelerations for 45 of the 100 design cases produced peak values less that the 150-g limit. As expected, the yield stress of the side pad was the most influential parameter for this impact location. A plot of the maximum acceleration in relation to the side pad yield stress, given in Fig. 15, shows that decreasing the yield stress reduces the maximum acceleration. The maximum headform accelerations of the front, crown, and side impact locations all benefit from lower values of side pad yield stress. The lower and upper bounds of the yield stress for the side pad are therefore set to 0.05 and 1.0 MPa, respectively, to increase the likelihood of peak accelerations near or below the 150-g limit for these three cases.

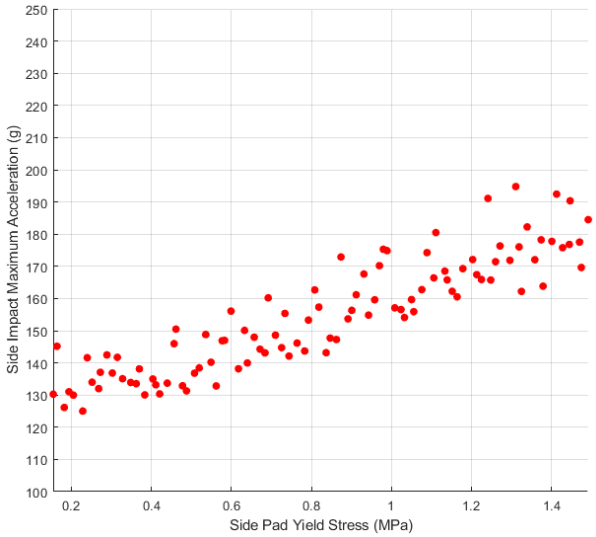


**Fig. 15 Maximum acceleration prediction of side impact vs. side pad yield stress**

## 6. Optimized Pad Parameters

A final 100-case space filling design was generated using the following parameter ranges: all initial pad moduli 5 to 33.3 MPa, front pad yield stress 0.15 to 1.5 MPa, crown pad yield stress 0.05 to 0.4 MPa, side pad yield stress 0.05 to 1.0 MPa, and nape and rear pad yield stresses restricted to a triangular area in the two-parameter design space bounded by the lines $\sigma_{ys,n} = 0.15$ MPa, $\sigma_{ys,r} = 0.15$ MPa, and $\sigma_{ys,r} = 1.20 - \sigma_{ys,n}$ MPa. Impact simulations at all five locations were completed, and the results were postprocessed to extract maximum headform accelerations. None of the design cases were able to meet the objective of maximum accelerations below 150 g for all impact locations due to the high predicted peak values produced by the front impact location. Achieving the lowest possible peak acceleration at a single impact location would reduce the severity of injury, but the results of these simulations suggest that tradeoffs between the impact locations are necessary to get closer to targeted limit of 150 g.

An evaluation criteria was created to determine the best performing set of input parameters with these tradeoffs in mind. This criteria focuses on achieving the goal of peak accelerations below the 150-g limit but does not provide an incentive for going below this limit. A score at each location is calculated, and the sum of the scores from all five locations is used to rank the design case with lower scores indicating the better performers. For the nape, rear, crown, and side impact locations, the location score $S_L$ is calculated using the following equation:

$$S_L = \begin{cases} 0 & if\ a_L \leq 150 \\ \frac{(a_L - 150)}{25} & if\ a_L > 150 \end{cases}, \quad (1)$$

where $a_L$ is the peak headform acceleration in g's for the design case at a particular location. This equation ensures that achieving the targeted acceleration is desirable, but going below the 150-g limit is not rewarded. For peak accelerations greater than 150 g, the score is normalized by 25 g to aid in postprocessing. The score of the front impact location for this criteria is calculated in relation to the minimum predicted peak acceleration $a_{min}$ at this location, which was 174.1 g. This difference is necessary because when comparing the peak acceleration for a case at this location with the targeted 150-g limit, the performance of the front impact location became more influential in the total score than the other four impact locations. The equation for the front location is therefore given by

$$S_L = \frac{(a_L - a_{min})}{25}. \tag{2}$$

The score for each of the design cases was calculated, and those with the lowest scores were collected for evaluation. The input parameters and resulting peak headform predictions are given in Table 1 for the five best performing (lowest scoring) design cases. The evaluation criteria provides a clear best performing case, as its score is significantly less than the second best performer and the difference between first and second place is nearly twice as great as between second and fifth. Polar plots of the pad yield stresses and initial moduli are provided in Fig. 16 to illustrate trends in the response of the pads that are beneficial to the overall performance in impact testing. These plots show that lower values of yield stresses for both the crown and side pads contribute to overall improvements in the predicted performance of the impact response. The front pad yield stresses for the best performing cases are greater than approximately 1 MPa, suggesting that ideal performance in the crown impact location must be sacrificed to improve the response from the front impact. This analysis also suggests that nape pad yield stresses in the higher end of the range are also desirable. A significant influence from the initial pad modulus was not seen in the results from any of the impact locations, although Fig. 16b suggests that a higher crown and nape pad modulus may be beneficial.

**Table 1 Five best performing cases ranked by lowest score**

| Pad input properties (MPa) | | | | | | | | | | Peak headform acceleration (g) | | | | | Score |
|---|---|---|---|---|---|---|---|---|---|---|---|---|---|---|---|
| $\sigma_{ys,n}$ | $E_{0,n}$ | $\sigma_{ys,r}$ | $E_{0,r}$ | $\sigma_{ys,s}$ | $E_{0,s}$ | $\sigma_{ys,f}$ | $E_{0,f}$ | $\sigma_{ys,c}$ | $E_{0,c}$ | Nape | Rear | Side | Front | Crown | |
| 0.96 | 18.68 | 0.15 | 6.27 | 0.16 | 13.29 | 1.19 | 6.95 | 0.06 | 32.52 | 152.3 | 158.6 | 133.0 | 184.6 | 137.0 | 0.86 |
| 0.76 | 6.81 | 0.28 | 12.89 | 0.46 | 16.69 | 1.05 | 11.25 | 0.07 | 7.93 | 152.1 | 155.0 | 140.3 | 191.5 | 155.4 | 1.20 |
| 0.76 | 20.38 | 0.42 | 10.61 | 0.09 | 20.13 | 1.36 | 17.23 | 0.08 | 28.45 | 136.0 | 168.0 | 127.2 | 184.1 | 152.9 | 1.24 |
| 0.62 | 28.74 | 0.55 | 7.27 | 0.07 | 13.62 | 1.15 | 17.58 | 0.13 | 32.22 | 140.1 | 174.6 | 130.7 | 174.4 | 157.5 | 1.30 |
| 0.82 | 14.27 | 0.15 | 21.75 | 0.13 | 7.71 | 0.96 | 9.33 | 0.09 | 28.62 | 165.6 | 159.0 | 130.7 | 183.3 | 146.1 | 1.35 |

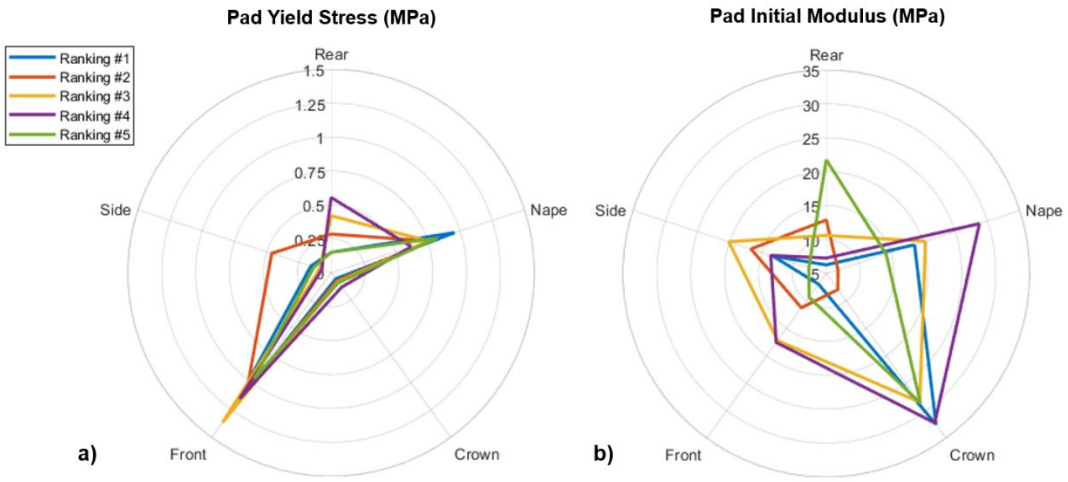


**Fig 16 Polar plots of pad specific inputs of a) yield stress and b) initial modulus for five best performing cases**

The results of this analysis suggest that there is a tradeoff between two pairs of impact locations. The response from nape and rear impacts are interrelated, with the reduction of peak accelerations from one location resulting in an increase in the other. This is the case for the front and crown impact locations as well. Balancing these competing forces in relation to the objectives is subjective. In this analysis, proximity to the targeted 150-g limit for all locations was given priority over exceptional performance at a single location.

Figure 17 plots the stress–strain curves of the optimized pad response along with the measured response of the Team Wendy pad. The responses of the rear, crown, and side pads are in the same regime as the Team Wendy response with a low yield stress before densification. The relationship between the rear and nape pads requires the yield stress of the nape to increase as a result of the lower rear pad yield stress. The higher yield stress of the front pad is needed to reduce the peak headform accelerations from the front impact.

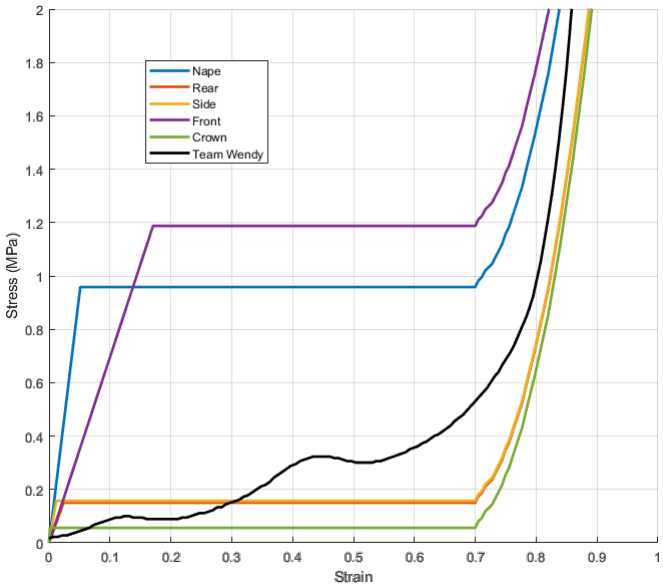


**Fig. 17 Stress vs. strain response of Team Wendy and optimized pads**

The predicted headform acceleration versus time curves for the baseline ACH model with Team Wendy pad properties are compared with the predicted optimized response for the five impact locations in Fig. 18. Significant reductions in peak acceleration are seen in the nape, rear, and front impact locations with smaller improvement in the side and crown impacts. The shape of the acceleration curve is modified most significantly in the nape and front impacts, where the accelerations ramp up more quickly and stay elevated over a longer period of time. The other impact locations also see a slightly steeper rise in the predicted acceleration, but generally level off and eliminate the peaks of the baseline response.

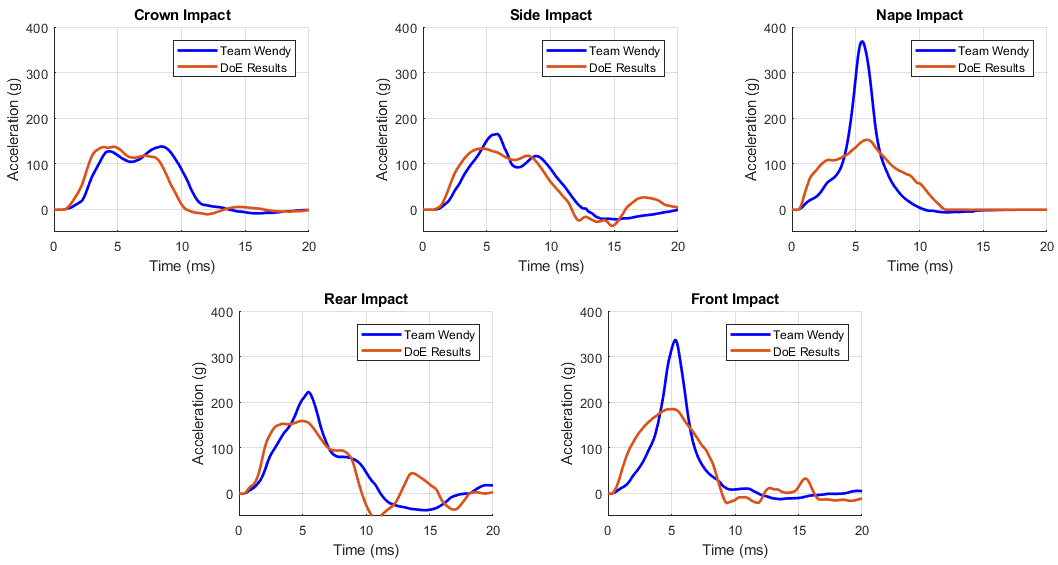


**Fig. 18 Comparison of baseline ACH model with Team Wendy pads and ACH model with optimized pads for the five impact locations**

## 7. Analysis with LS-OPT

Optimization of the pad material response using the DOE methods detailed in the previous sections did not result in the desired outcome of peak headform accelerations below the 150-g limit for all five impact locations. An additional method to potentially solve this problem was explored with the use of the model optimization software LS-OPT. LS-OPT is a standalone design optimization and probabilistic analysis package with an interface to LS-Dyna.[11] The software was used to run a sequential meta-model-based optimization with selective domain reduction. The objective of the optimization was to minimize the peak predicted headform accelerations from each impact location simultaneously. The optimization methodology, shown in Fig. 19, creates a D-optimal design within the initial parameter space, simulates the five helmet impacts, extracts the maximum headform accelerations, and fits a meta-model to the combined results. Using the meta-model, an optimal case is predicted and its corresponding input parameters are selected. The ranges for each input parameter are adjusted around these values, and the optimization process is repeated. This process continues until the finite element modeling results do not change significantly from iteration to iteration, or a set number of iterations are completed (in this case, the maximum number of iterations is set to 12 to limit the computational expense of the optimization).

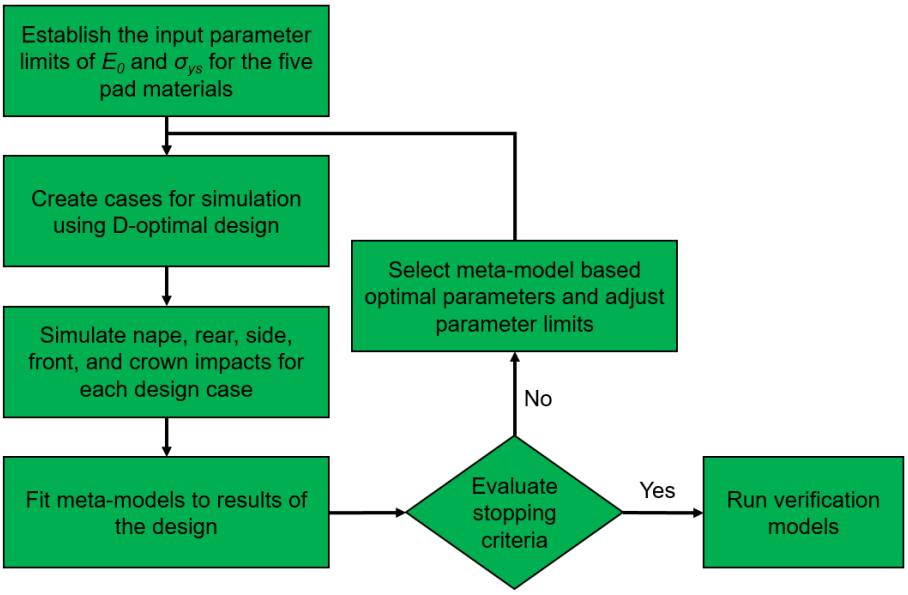


**Fig. 19 Flowchart for pad material optimization with LS-OPT**

The pad material optimization problem was created and simulated with LS-OPT version 5.1.1. The lower and upper limits of the initial pad modulus $E_0$ were set to the same values used in the previous analysis, at 5 and 33.3 MPa, respectively. Different limits for pad yield stress were used in this analysis based on knowledge from the previous approach. The adjusted limits also allow the optimization algorithm to explore a wider range of yield stresses for a potential optimal solution in some cases. The limits used were 0.15 to 1.5 MPa for nape and rear yield stresses, 0.01 to 1.5 MPa for the crown and side yield stresses, and 0.5 to 1.5 MPa for the front yield stress. The optimization algorithm was run over 12 iterations with a 17-case D-optimal design created at each iteration. Once the analysis was completed, the results were further postprocessed for comparison with the previous analysis. The progression of the minimum total score, as calculated with Eqs. 1 and 2, is shown in Fig. 20. The previous minimum total score was 0.86, and the lowest total score found using in the LS-OPT analysis is 0.26, a significant improvement.

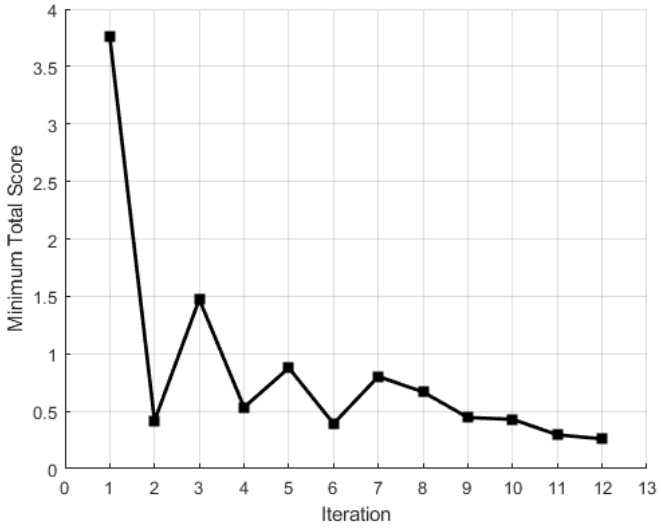


**Fig. 20 Progression of lowest total score per LS-OPT optimization iteration**

Table 2 shows the input parameters and maximum headform accelerations predicted for the five best performing design cases from the LS-OPT analysis. The input parameters for the best performing cases are within a relatively narrow range of values due to the selective domain reduction of the optimization procedure. In this analysis, 23 cases (out of a total of 204) were found where the peak headform acceleration from the nape, rear, side, and crown impacts were below 150 g and the acceleration from the front impact was below 185 g. This solution set was not identified by the previous DOE optimization scheme, though in theory it could have been found if the parameter space had not been down-selected and at greater computational expense, as described in the following.

**Table 2 Five best performing cases from LS-OPT analysis ranked by lowest score**

| Pad input properties (MPa) | | | | | | | | | | Peak headform acceleration (g) | | | | | Score |
|---|---|---|---|---|---|---|---|---|---|---|---|---|---|---|---|
| $\sigma_{ys,n}$ | $E_{0,n}$ | $\sigma_{ys,r}$ | $E_{0,r}$ | $\sigma_{ys,s}$ | $E_{0,s}$ | $\sigma_{ys,f}$ | $E_{0,f}$ | $\sigma_{ys,c}$ | $E_{0,c}$ | Nape | Rear | Side | Front | Crown | |
| 0.51 | 8.91 | 0.42 | 26.66 | 0.08 | 11.87 | 1.08 | 11.65 | 0.01 | 11.92 | 148.6 | 141.5 | 128.0 | 178.6 | 132.3 | 0.26 |
| 0.54 | 9.74 | 0.44 | 26.13 | 0.11 | 13.26 | 1.03 | 13.48 | 0.01 | 13.09 | 142.8 | 145.0 | 126.8 | 179.5 | 134.9 | 0.29 |
| 0.57 | 10.57 | 0.42 | 26.13 | 0.14 | 11.87 | 1.08 | 11.65 | 0.02 | 11.92 | 142.3 | 146.7 | 125.0 | 180.5 | 135.6 | 0.33 |
| 0.54 | 11.40 | 0.40 | 24.37 | 0.17 | 10.49 | 1.03 | 13.48 | 0.01 | 13.09 | 148.2 | 142.2 | 121.8 | 181.7 | 136.0 | 0.38 |
| 0.57 | 8.91 | 0.42 | 25.60 | 0.14 | 10.49 | 1.08 | 9.83 | 0.01 | 14.27 | 142.8 | 146.3 | 125.2 | 181.7 | 132.1 | 0.38 |

This difference in results between the solution sets identified by the DOE method versus that of LS-OPT can be attributed to the significance of the initial modulus. In the DOE analysis there was no apparent influence from the initial modulus values on peak headform accelerations for any of the impact locations. The initial modulus of the pads for the best performing cases also do not have any significant trends, as shown in Fig. 16b. This contrasts with the best performing cases in the LS-OPT analysis shown in Fig. 21. Any interactions between two or more of the 10 input parameters are difficult to identify through a manual process like the DOE method.

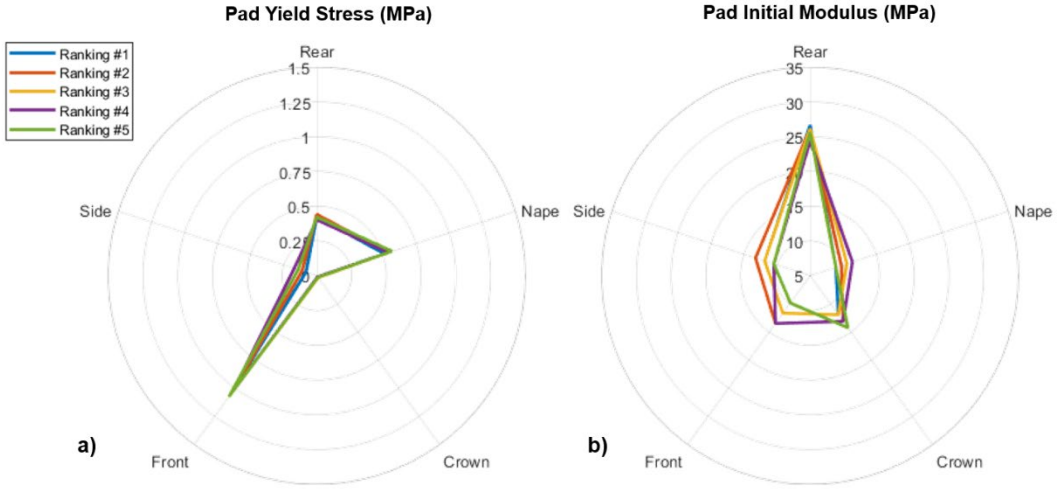


**Fig. 21 Polar plots of pad specific inputs of a) yield stress and b) initial modulus for five best performing cases from the LS-OPT analysis**

## 8. Comparison of Analysis Results

A comparison of the headform acceleration versus time curves for the baseline Team Wendy pads, the optimized pads from the DOE analysis, and the optimized pads from the LS-OPT analysis are shown in Fig. 22. The LS-OPT analysis produced predictions that reduce the peak accelerations for each impact in comparison with the DOE optimized results, although the predicted shapes of the curves are not significantly different.

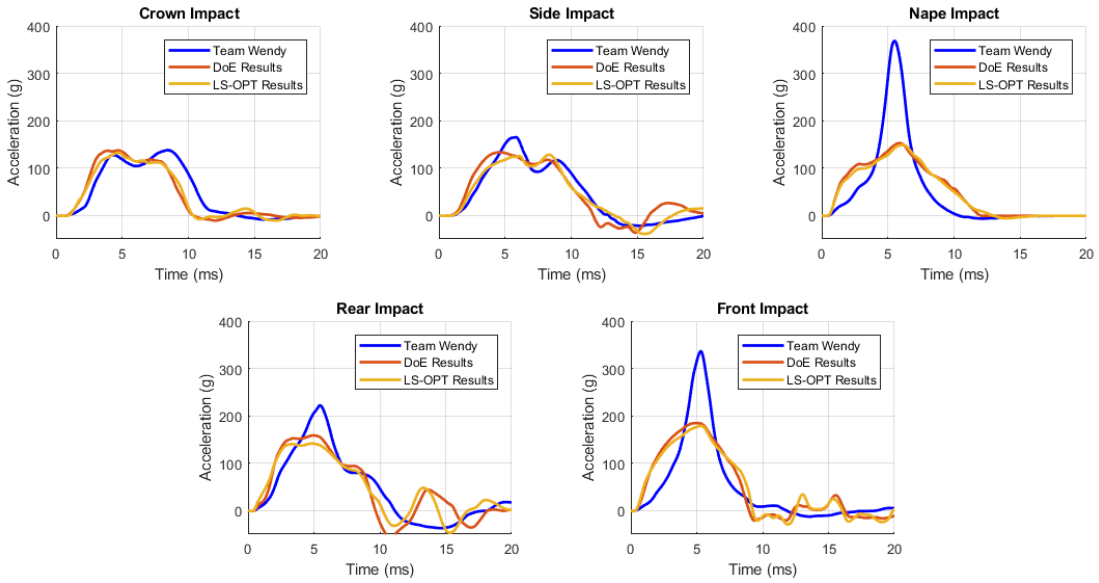


**Fig. 22 Comparison of acceleration vs. time curves for Team Wendy, DOE optimized pads, and LS-OPT optimized pads**

The pad responses for the optimized results of the DOE and LS-OPT analyses are shown in Fig. 23. The optimal pad properties found manually with the DOE analysis for the side, front, and crown pad are similar to the resulting optimized properties from LS-OPT. The optimal nape and rear yield stresses found with LS-OPT are within the ranges of values corresponding to lower peak accelerations found in the previous analysis (Fig. 7), although the LS-OPT analysis identified a combination of initial pad moduli that further reduced these peak values.

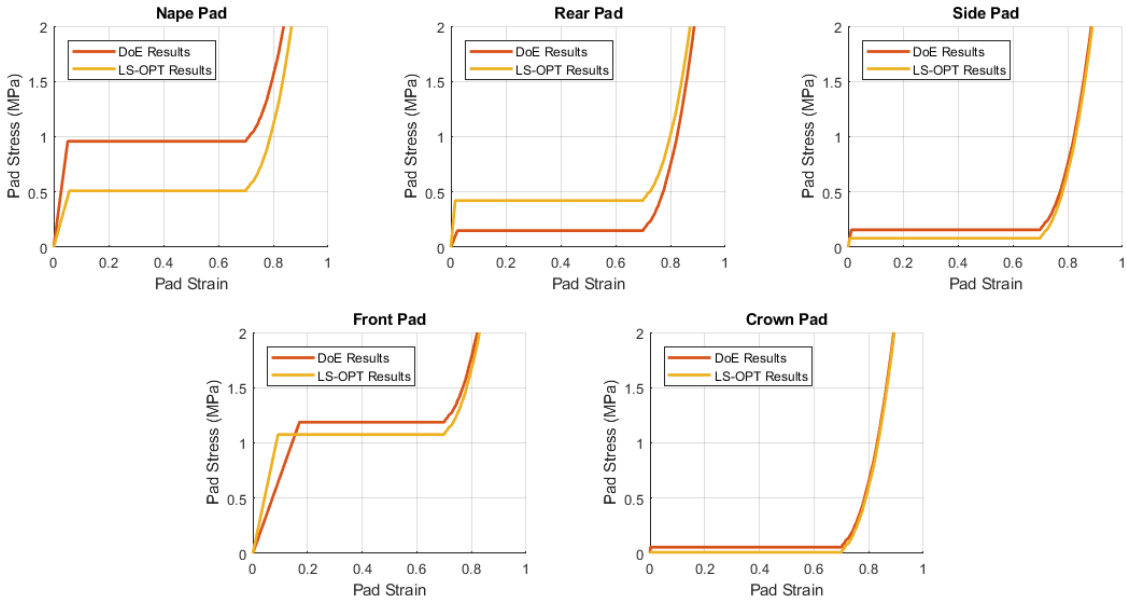


**Fig. 23 Comparison of optimized pad material response for DOE and LS-OPT analyses**

## 9. Conclusions

A previously developed and experimentally correlated model of the ACH helmet and suspension system was used to study the influence of pad material response on the predicted peak headform accelerations when subjected to low-velocity impact. Ten input parameters defining the pad material response of the five individual pad groups were optimized with the objective of reducing peak headform accelerations below 150 g for the system subjected to impacts in the nape, rear, side, front, and crown locations. A series of space filling designs were created to explore the parameter space and determine which critical aspects of the assumed pad response contributed to the reduction of peak accelerations. Although no cases were found that reduced accelerations below the 150-g limit for all five impact locations, a set of input parameters was identified that reduced the predicted peak accelerations significantly below the baseline levels. The resulting compression response of each pad location around the helmet is unique to that location in order to achieve optimal performance. Therefore, the optimized result is implicitly higher performing than a single material solution. Note that this optimization was performed without regard for other important characteristics of helmet suspension systems such as comfort, which is inherently difficult to quantify due to individual preference. Additional experimentation will be necessary to confirm the outcome of this analysis, but these results provide a guideline for ACH padding selection to limit the severity of head injury resulting from blunt force impact.

## 10. References


1. Mills NJ. Polymer foams handbook: engineering and biomechanics applications and design guide. Oxford (England): Butterworth-Heinemann; 2007.

2. McEntire BJ, Whitley P. Blunt impact performance characteristics of the advanced combat helmet and the paratrooper and infantry personnel armor system for ground troops' helmet. Fort Rucker (AL): Army Aeromedical Research Laboratory (US): 2005.

3. Spinelli DJ, Plaisted TA, Wetzel ED. Adaptive head impact protection via a rate-activated helmet suspension. Mater Design. 2018;54:153–169.

4. Purchase description - helmet, advanced combat (ACH): AR/PD 10-02 rev A. Ft Belvoir (VA): Program Executive Office Soldier; 2012.

5. US Department of Transportation (DOT). Laboratory test procedure for FMVSS No. 218 motorcycle helmets. Washington (DC): DOT; 2011 May 13. p. 33.

6. Council NR. Review of Department of Defense test protocols for combat helmets. Washington (DC): The National Academies Press; 2014. p. 158.

7. Bricknell MC, Craig SC. Military parachuting injuries: a literature review. Occup Med Lond. 1999;49(1):17–26.

8. Plaisted T, Staniszewski J, Choi H, Zhang T, Boyd S, Green W. Development of the low-velocity advanced combat helmet (LVACH) model for blunt impact head injury research. Aberdeen Proving Ground (MD): Army Research Laboratory (US); 2018. p. 60.

9. Bruggeman M. Blunt impact testing procedure for combat helmets: IOP number: ATC-MMTB-029 rev E. Aberdeen Proving Ground (MD): Aberdeen Test Center Warfighter Directorate; 2013. p. 25.

10. Begley MR, Zok FW. Optimal material properties for mitigating brain injury during head impact. J Appl Mech. 2013;81(3):031014–031014-5.

11. Stander N, Roux W, Basudhar A, Eggleston T, Goel T, Craig K. LS-OPT user's manual. Livermore (CA): Livermore Software Technology Corporation; 2008.

## List of Symbols, Abbreviations, and Acronyms

| | |
|---|---|
| ACH | Advanced Combat Helmet |
| CORA | CORrelation and Analysis |
| DOE | Design of Experiments |
| DOT | US Department of Transportation |
| FMVSS | Federal Motor Vehicle Safety Standard |
| g | gravity force |
| LVACH | Low-Velocity Advanced Combat Helmet |
| ZAP | Zorbium Action Pad |

| | |
|---|---|
| 1 (PDF) | DEFENSE TECHNICAL INFORMATION CTR DTIC OCA |
| 1 (PDF) | CCDC ARL FCDD RLD CL TECH LIB |
| 1 (PDF) | GOVT PRINTG OFC A MALHOTRA |
| 1 (PDF) | CCDC ARL FCDD RLW MA J STANISZEWSKI |